Journal of Power Sources 203 (2012) 274–281

Contents lists available at SciVerse ScienceDirect

Journal of Power Sources

journal homepage: www.elsevier.com/locate/jpowsour

# High performance dye-sensitized solar cells based on platinum nanoparticle/multi-wall carbon nanotube counter electrodes: The role of annealing

Kuan-Chieh Huang[a], Ying-Chiao Wang[b], Po-Yen Chen[a], Yi-Hsuan Lai[a], Jen-Hsien Huang[c], You-Han Chen[a], Rui-Xuan Dong[b], Chih-Wei Chu[c,d], Jiang-Jen Lin[b,*], Kuo-Chuan Ho[a,b,**]

[a] Department of Chemical Engineering, National Taiwan University, Taipei 10617, Taiwan
[b] Institute of Polymer Science and Engineering, National Taiwan University, Taipei 10617, Taiwan
[c] Research Center for Applied Sciences, Academia Sinica, Taipei 11529, Taiwan
[d] Department of Photonics, National Chiao Tung University, Hsinchu 300, Taiwan

ARTICLE INFO

*Article history:*
Received 3 June 2011
Accepted 15 November 2011
Available online 23 November 2011

*Keywords:*
Annealing
Dye-sensitized solar cell
Multi-wall carbon nanotube
Platinum nanoparticle
Surface roughness

ABSTRACT

A composite film is coated on the FTO using a solution, containing a synthesized dispersant, poly(oxyethylene)-segmented imide (POEM), dihydrogen hexachloroplatinate ($H_2PtCl_6$), and multi-wall carbon nanotube (MWCNT); the thus coated FTO is used as the counter electrode (CE) for a dye-sensitized solar cell (DSSC). The annealing temperature of the composite film, in the range of 110–580 °C, is found to be crucial for optimizing its catalytic ability to obtain the best possible performance for the DSSC. About 47% loss in mass for the POEM/$H_2PtCl_6$/MWCNT composite is observed from 110 to 390 °C, due to not only the progressive formation of PtNPs from $H_2PtCl_6$ but the decomposition of POEM. Therefore, the efficiencies ($\eta$) of DSSCs applying these CEs are enhanced from 1.28 ± 0.08% (110 °C) to 8.47 ± 0.21% (390 °C). The mass of the composite loses dramatically under heating above 390 °C, due to the decomposition of MWCNTs. The $\eta$ decreases to 7.77 ± 0.15% at 450 °C because the decrease in surface roughness of film. PtNPs grow in sizes from 450 to 580 °C, resulting in the further decrease in catalytic ability of film and the observed $\eta$ from 7.77 ± 0.15% to 7.19 ± 0.21%.



## 1. Introduction

The counter electrode (CE), a key component in a dye-sensitized solar cell (DSSC), has the essential function of conversion of triiodide ($I_3^-$) into iodide ($I^-$) in the electrolyte of the cell, and thereby completes the cycle of operation of the cell [1,2]. Due to its extraordinary catalytic ability and conductivity, platinum (Pt), is usually employed as the catalytic film on the conducting substrate of a CE. The platinized CE not only reduces the voltage loss, resulting from the charge-transfer overpotential at it, but also reflects the light falling on it [3]. Therefore, a Pt-based CE is of pivotal importance for a high performance DSSC. Several techniques, such as magnetron sputtering, electro-deposition, and thermal decomposition have been employed for the deposition of a Pt film on the CE substrate of a DSSC [4–7]. Papageorgiou et al. [6] have reported about a high performance DSSC; the CE of the pertinent cell was coated with a nanoparticles-film of Pt, through thermal decomposition. The catalytic Pt films, consisting of platinum nanoparticles (PtNPs) were obtained from the Pt precursor, dihydrogen hexachloroplatinate ($H_2PtCl_6$) [8].

Recently, some carbon materials and conducting polymers were used as efficient catalysts on the CEs of DSSCs [9,10]. Carbon nanotubes (CNTs) have long since been explored as promising materials in electrochemistry, owing to their electrical, mechanical, and thermal properties [11,12]. CNTs are efficient catalysts for $I_3^-$ reduction in a DSSC; such cells exhibit a competitive performance, with reference to the DSSCs based on Pt CEs [13–17]. We have prepared a nanocomposite film for a CE by using a synthesized polymer, poly(oxyethylene)-segmented imide (POEM); the film consisted of PtNPs and multi-wall CNTs (MWCNTs) [18].

The present work deals with a DSSC, consisting of a CE with a catalytic layer of PtNP/MWCNT. Because of the coexistence of three components in the deposition solution, i.e., $H_2PtCl_6$, MWCNTs, and POEM, we determined most suitable annealing temperature for PtNP/MWCNT-coated CE. The variations in the catalytic film, e.g., surface morphology, crystalline size of the PtNPs, amount of POEM

* Corresponding author at: National Taiwan University, Institute of Polymer Science and Engineering, No. 1, Sec. 4, Roosevelt Rd., Taipei 10167, Taiwan. Tel.: +886 2 3366 5312; fax: +886 2 8369 1384.
** Corresponding author at: National Taiwan University, Department of Chemical Engineering, No. 1, Sec. 4, Roosevelt Rd., Taipei City 10617, Taiwan. Tel.: +886 2 2366 0739; fax: +886 2 2362 3040.
*E-mail addresses:* jianglin@ntu.edu.tw (J.-J. Lin), kcho@ntu.edu.tw (K.-C. Ho).

0378-7753/$ – see front matter © 2011 Elsevier B.V. All rights reserved.
doi:10.1016/j.jpowsour.2011.11.031

in the film, and consequent variation in the power-conversion efficiency ($\eta$) of the pertinent cell, due to the variation in the annealing temperature of the catalytic film, are studied. The DSSC assembled with the PtNP/MWCNT-CE, in which the CE was annealed at the optimal temperature, has shown an $\eta$ of $8.47 \pm 0.21\%$. The nanocomposite film was characterized at various annealing temperatures, using spectroscopic and electrochemical techniques.

## 2. Experimental

### 2.1. Materials

MWCNTs (diameter = 40–60 nm, length = 0.5–10 μm) were received from Seedchem Company Pty., Ltd., Melbourne Vic, Australia. $H_2PtCl_6$ (ACS regent, Premion, 99.95%) and sodium borohydride ($NaBH_4$, 98%) were purchased from Alfa Aesar Chemical Co. Anhydrous LiI, $I_2$, acetonitrile (ACN) and poly(ethylene glycol) (PEG, M.W. = 20,000 g mol$^{-1}$) were received from Merck. Titanium(IV) isopropoxide (TTIP, +98%), 4-*tert*-butylpyridine (TBP, 96%), and *tert*-butanol (TBA, 99.5%) were obtained from Acros. 3-methoxypropionitrile (MPN, 99%) was a product from Fluka. *cis*-Bis(isothio-cyanato)bis(2,2′-bipyridyl-4,4′-dicarboxylato)ruthenium(II)bis- tetrabutylammonium (so-called N719), and 1,2-dimethyl-3-propylimidazolium iodide (DMPII) were obtained from Solaronix S.A., Aubonne, Switzerland.

### 2.2. Preparation of nanocomposite PtNP/MWCNT counter electrode

Poly(oxyethylene)-segmented imide polymer (POEM) was synthesized by mixing poly(oxyethylene)-diamine (POE2000, M.W. = 2000 g mol$^{-1}$, waxy solid, melting point = 37–40 °C, amine content 0.95 meq. g$^{-1}$ with an average 39 oxyethylene and 6 oxypropylene units in the structure) and 4,4′-oxydiphthalic anhydride (ODPA, 97% purity, Aldrich Chemical Co.). The use of POE-backboned polymer dispersant allows the non-covalent blending of PtNPs with MWCNTs; the amphiphilic solvating property of POEM is required for high dispersibility of PtNP/MWCNT composite in the solution. The POEM polymer was synthesized through the reaction of POE2000 with ODPA at a molar ratio of 6:5; the following procedure is adopted. POE2000 (10.00 g, 5 mmol) in tetrahydrofuran (THF, TEDIA Company Inc.) (15 mL) was poured into a 100 mL three-necked, round-bottomed flask, equipped with a magnetic stirrer, nitrogen inlet-outlet lines, and a thermometer; a solution of ODPA (1.29 g, 4 mmol) in THF (10 mL) was added to the reactor through a funnel in a drop-wise manner. During the addition, the mixture was stirred vigorously and the reactor was maintained at 150 °C for 3 h. The product was subjected to rotary evaporation under a reduced pressure and was finally recovered as a yellowish waxy solid. During the process, samples were taken periodically and characterized by using a Fourier transform infrared (FTIR) spectroscopy. The FTIR spectra shows that the absorption peaks of anhydride at 1780 cm$^{-1}$ (s) and 1850 cm$^{-1}$ (w) disappeared at the expense of the peaks at 1713 and 1773 cm$^{-1}$ for the asymmetric stretch of imide. The characteristic absorption of oxyalkylene was observed at 1100 cm$^{-1}$. The combination of PtNPs with MWCNTs was accomplished through an *in situ* reduction of $H_2PtCl_6$ in the presence of MWCNTs in the dispersant POEM in an aqueous medium. The MWCNTs (0.036 g) were first dispersed in 7.11 g of deionized water in a vial and sonicated under a VCX 500 Ultrasonicator at ambient temperature for 15 min. The resulting solution was dark black with some solid precipitate at the bottom of the container, indicating a low degree of dispersion. In a separate glass container, POEM (1.0 g) and $H_2PtCl_6$ (1.00 g, 2.4 mmol) were dissolved in 5.14 g of deionized water, and the contents were added to a solution of MWCNTs/deionized water (7.11 g). A homogenous suspension of MWCNTs was obtained by mixing them in the presence of POEM and $H_2PtCl_6$. PtNPs were then generated by slowly adding 0.7 wt% of $NaBH_4$ (0.007 g) into 1 g deionized water (due to the reduction of $H_2PtCl_6$). This dispersion was further stirred for several hours at ambient temperature and monitored for the attachment of PtNPs on the surfaces of MWCNTs, using a transmission electron microscopy (TEM). The prepared solution was then spin-coated on a fluorine-doped $SnO_2$ glass substrate (FTO, surface resistance = 15 Ω sq.$^{-1}$, Solaronix S.A., Aubonne, Switzerland), in which 2000 rpm were used for 30 s. FTO glasses coated with the nanocomposite films were annealed at various temperatures of 110, 200, 390, 450, and 580 °C for 20 min. Thus, the fabrication of PtNP/MWCNT counter electrode (PtNP/MWCNT-CE) was accomplished.

### 2.3. Preparation of $TiO_2$ photoanode and assembly of DSSC

In a sol–gel method, the TTIP was added into $H_2O/HNO_3$ at 88 °C for 8 h. The resultant solution was further subjected to 240 °C in an autoclave for 12 h to obtain nanocrystalline $TiO_2$. The $TiO_2$ solution was concentrated to 13 wt%. 30 wt% of PEG (with respect to $TiO_2$) was then added to the slurry. The paste was then doctor-bladed on the FTO, and the $TiO_2$/FTO was further annealed at 450 °C for 30 min. After repeating the coating and annealing twice, a light scattering layer (a layer of $TiO_2$ with particles of 300 nm) was coated on the $TiO_2$ film; the film was then again annealed at 450 °C for 30 min [19]. The $TiO_2$ film was shaved to obtain an active area of 0.16 cm$^2$, and then it was immersed in a solution of 0.3 mM N719 in ACN/TBA (equal volume) for 12 h. The dye-adsorbed $TiO_2$ photoanode was attached to a CE, using a 25 μm-thick Surlyn film as the spacer between the electrodes. The MPN-based liquid electrolyte containing 0.6 M DMPII, 0.1 M LiI, 0.05 M $I_2$, and 0.5 M TBP was then injected into the space separated by the Surlyn film (through the capillary effect).

### 2.4. Instrumentation

Thermo-gravimetric analyzer (TGA, TGA-7, PerkinElmer) was used for quantifying the loss in the weight percentage of the samples. The surface morphologies of the CEs were observed by field-emission scanning electronic microscopy (FE-SEM, Zeiss EM 902A). Energy dispersive spectrometer (EDS, NovaTM NanoSEM 230) and atomic force microscopy (AFM, NanoScope) equipped with a probe of tapping mode were used for estimating the contents of chlorine and the surface roughness of the CEs, respectively. The crystalline orientations and sizes of PtNPs were measured and calculated from X-ray diffraction (XRD, Philips, X'Pert) patterns. Cyclic voltammetry (CV, CHI, electrochemical workstation, model 440) was performed with a three-electrode cell for determining the active surfaces of the films. Surface of the DSSC was illuminated by a class A quality solar simulator (PEC-L11, AM 1.5G, Peccell Technologies, Inc.) and the incident light intensity (100 mW cm$^{-2}$) was calibrated with a standard Si cell (PECSI01, Peccell Technologies, Inc.). Photoelectrochemical characteristics of the DSSC were recorded with a potentiostat/galvanostat (PGSTAT 30, Autolab, Eco-Chemie, the Netherlands). Electrochemical impedance spectra (EIS) were obtained by the above-mentioned potentiostat/galvanostat equipped with an FRA2 module, under a constant light illumination of 100 mW cm$^{-2}$.

## 3. Results and discussion

The synthesized POEM dispersant has the chemical structure shown in Fig. 1. POEM was used for dispersing the inorganic

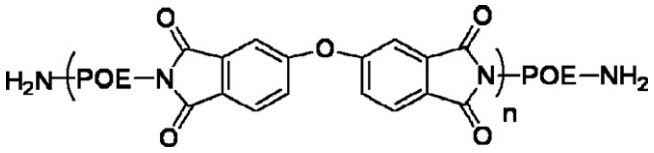


**Fig. 1.** The chemical structure of POEM.

components and also for preventing the self-aggregation of MWCNTs in the aqueous solution, containing $H_2PtCl_6$ and $NaBH_4$. In the presence of an excess amount of $H_2PtCl_6$ with respect to $NaBH_4$ (weight ratio of 143:1), a partial formation of PtNPs occurs, implying that $Pt^{4+}$ is partially reduced to $Pt^0$ in the solution [20]. The residual $H_2PtCl_6$ in the solution would, however decomposes to Pt during the annealing processes [7,8].

The mass of the solidified composite, POEM/$H_2PtCl_6$/MWCNT, prepared from the above solution through the help of a freeze dryer, depends on the annealing temperature, as shown in Fig. 2. Fig. 2 shows the residual masses of both POEM and MWCNT at different temperatures. The mass of the composite decreases as the annealing temperature increases from 110 to 390 °C. The loss in the mass of the composite can be attributed to the following chemical reaction, associated with the progressive formation of the Pt from $H_2PtCl_6$; in the chemical reaction, $Cl_2$ and $H_2O$ can be produced during the annealing process, as follows:

$$2H_2PtCl_6 + O_2 \rightarrow 2H_2O + 2Pt + 6Cl_2\uparrow \quad (1)$$

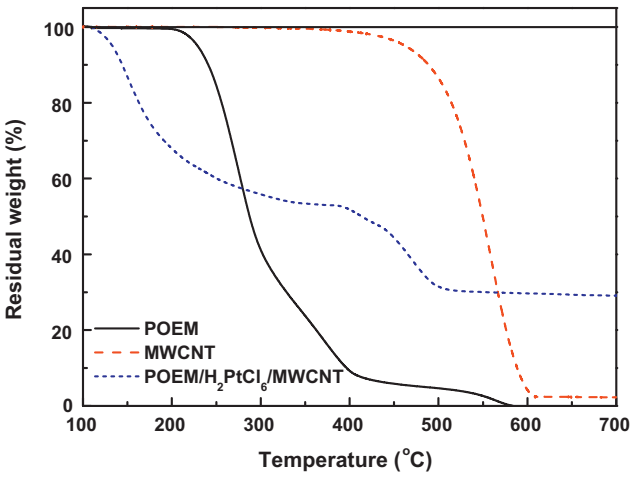


**Fig. 2.** TGA spectra of POEM, MWCNTs, and POEM/$H_2PtCl_6$/MWCNT.

The release of $Cl_2$ will be further evidenced (loss in the percentage of mass) through EDS analyses, to be discussed at a later stage. Another reason for the loss in the mass of the composite lies in the dramatic loss of the mass of POEM due to its decomposition at around 200 °C. When the annealing temperature is higher than 390 °C, the decomposition of MWCNT is responsible for the significant mass loss of the composite (Fig. 2). The mass of the composite

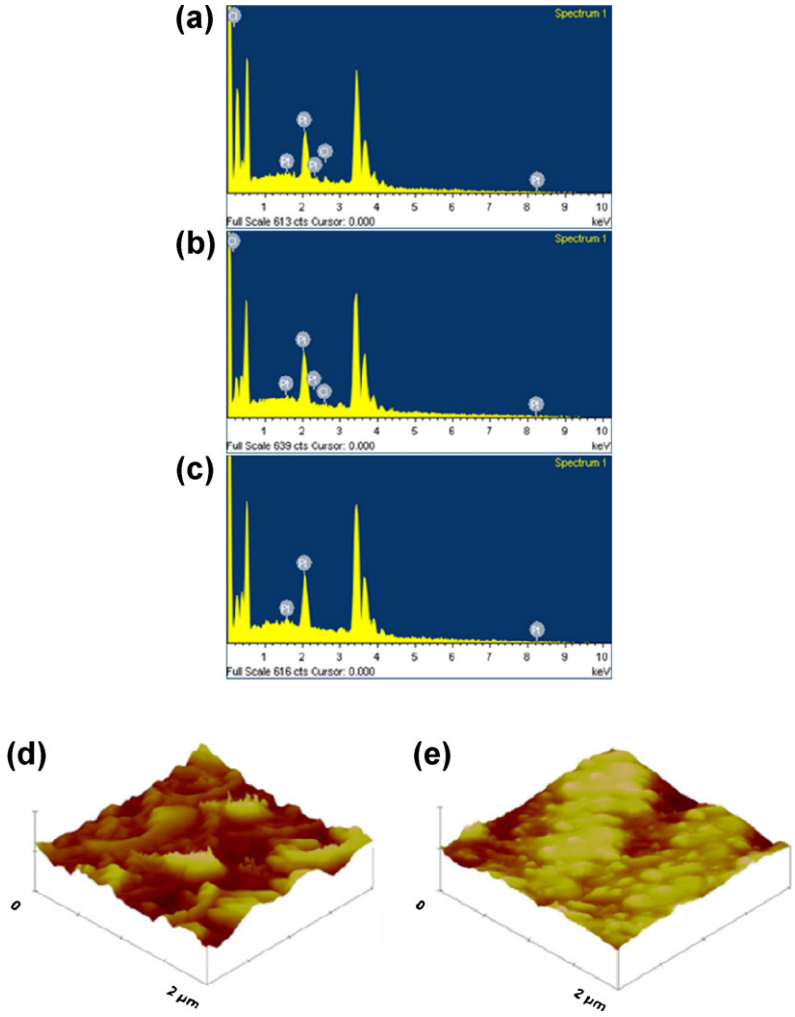


**Fig. 3.** EDS spectra of PtNP/MWCNT film annealed at (a) 110, (b) 200, and (c) 390 °C; AFM images of PtNP/MWCNT film annealed at (d) 390 and (e) 450 °C.

**Table 1**
Chlorine (Cl) in weight percentage and the corresponding root-mean-square roughness ($R_{ms}$) of the film of PtNP/MWCNT, annealed at various temperatures. The value at each temperature was an average of values obtained at three different surface locations.

| Annealing temp. | Cl (wt%) | $R_{ms}$ (nm) |
|---|---|---|
| 110 °C | 6.30 ± 0.73 | 21.55 ± 2.47 |
| 200 °C | 0.94 ± 0.82 | 24.12 ± 2.72 |
| 390 °C | 0.00 ± 0.00 | 22.66 ± 1.45 |
| 450 °C | 0.00 ± 0.00 | 14.97 ± 2.98 |
| 580 °C | 0.00 ± 0.00 | 14.30 ± 2.35 |

remains stable in the range of annealing temperature from 500 to 700 °C; the presence of metallic Pt may be attributed to this stable mass.

To find the reason for the decrease in the mass of the composite, as the annealing temperature increases from 110 to 390 °C, we have performed EDS analyses of the PtNP/MWCNT composite film at different temperatures, and the spectra are shown in Fig. 3a–c. The energy level at 2.62 keV represents the chlorine (Cl), which exhibits a decrease in intensity as the annealing temperature increases from 110 to 390 °C. This implies a gradual release of $Cl_2$ with the increase of the annealing temperature; the decrease in the Cl content was found to be from 6.30 ± 0.73 to 0.00 ± 0.00 wt%, as the annealing temperature had decreased from 110 to 390 °C (Table 1). Table 1 suggests that the $H_2PtCl_6$ is completely converted to Pt at 390 °C. In the range of 110–200 °C, the weight loss of Cl, calculated according to Eq. (1) using Fig. 2, is 7.64 wt%, which roughly agrees with the value obtained from the EDS data (5.36 wt%). For the range of 200–390 °C, however, the difference in weight losses calculated according to Eq. (1) using Fig. 2 (4.33 wt%) and obtained from the EDS data (0.94 wt%) is large. This weight loss of 4.33 wt% is not only due to the liberation of Cl from the conversion of $H_2PtCl_6$ to PtNP, but also due to the decomposition of POEM which occurs at around 200 °C (Fig. 2).

Root-mean-square roughness ($R_{ms}$) values of the composite films obtained from AFM are also shown in Table 1. The $R_{ms}$ values vary greatly at the annealing temperatures of 390 °C (22.66 ± 1.45 nm) and 450 °C (14.97 ± 2.98 nm). The AFM images of the films annealed at 390 and 450 °C are shown in Fig. 3d and e, respectively; the AFM images exhibit relatively rough and smooth surfaces at 390 and 450 °C, respectively. Rod-like structures are apparent in the film in Fig. 3d, and they may contain the MWCNTs; Fig. 3e does not show such structures, indicating that the MWCNTs have partially decomposed at 450 °C. The distinct change both in the surface morphology as well as in the $R_{ms}$ value of the composite film annealed at 390 and 450 °C is due to the partial decomposition of MWCNT at 450 °C; this phenomenon is also consistent with the behavior of the corresponding trace in the TGA diagram (Fig. 2). Fig. 4 shows the variations of Cl content (wt%) and $R_{ms}$ value for the PtNP/MWCNT film at 110, 200, 390, 450, and 580 °C. It can be seen that the Cl content becomes zero at the temperature of 390 °C. The value of $R_{ms}$ varies slightly in the temperature range of 110–390 °C, and again in the temperature range of 450–580 °C; the $R_{ms}$ values show a drastic decrease in the temperature range from 390 to 450 °C. The reason for this drastic change is the loss of MWCNT, as already mentioned.

It is clear that the PtNPs were formed, when the composite film was annealed. To understand the formation of PtNPs from $H_2PtCl_6$ and also the variation in the crystalline size of the thus formed PtNP, the presence and crystalline growth of PtNPs were studied by XRD (Fig. 5). In order to observe the changes in the crystalline sizes of PtNPs, without any interference due to POEM or MWCNTs, we have coated the substrates only using $H_2PtCl_6$ and subjected the Pt films obtained at different temperatures for XRD analyses. The crystallinity of Pt(1 1 1) is largest at 580 °C, as can be seen from

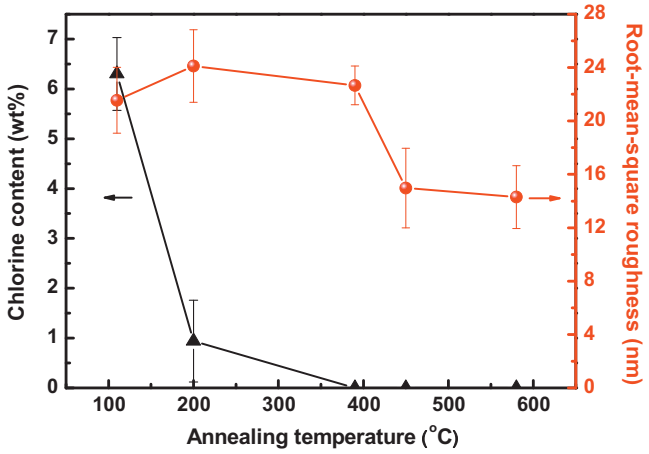


**Fig. 4.** Variations of Cl content (wt%) and root-mean-square roughness ($R_{ms}$) value of the PtNP/MWCNT film at 110, 200, 390, 450, and 580 °C.

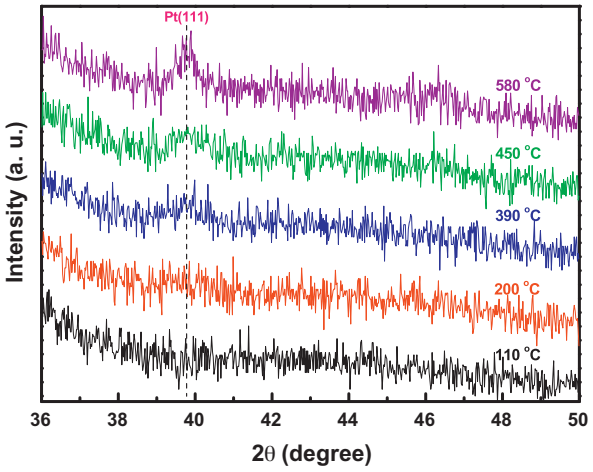


**Fig. 5.** XRD patterns of the PtNP films, annealed at various temperatures.

its 2$\theta$ value at 39.7° [21]. The crystalline size ($D$) can be calculated using the following Scherrer's equation

$$D = \frac{K\lambda}{\beta \cos\theta} \quad (2)$$

where $K$, $\lambda$, and $\theta$ are 0.89, 1.54 Å, and 39.7°/2, respectively, and $\beta$ is the width at half maximum of the diffraction peak corresponding to Pt(1 1 1) [22]. The values of $D$ at 390, 450, and 580 °C were found to be 6.63, 7.67, and 14.58 nm, respectively (Table 2). It has been reported that a growth in the crystalline size of PtNPs causes a decline in the catalytic ability of the pertinent film [23]. Therefore, the effect of crystalline size on the catalytic ability of the film

**Table 2**
Crystalline size ($D$) of platinum nanoparticle, ratio of real area to geometrical area, i.e., $A_{real}/A_{geometry}$ ($A_r/A_g$), interfacial charge-transfer resistances ($R_{ct1}$ and $R_{ct2}$), and exchange current density ($J_0$) of the DSSCs with PtNP/MWCNT-CEs, annealed at various temperatures. DSSCs were illuminated at 100 mW cm$^{-2}$.

| Annealing temp. | $D$ (nm) | $A_r/A_g$ | $R_{ct1}$ (Ω) | $R_{ct2}$ (Ω) | $J_0$ (mA cm$^{-2}$) |
|---|---|---|---|---|---|
| 110 °C | – | ND | 108.00 | 111.20 | 0.12 |
| 200 °C | ND[a] | 2.16 | 11.93 | 15.26 | 1.08 |
| 390 °C | 6.63 | 2.57 | 5.73 | 15.64 | 2.24 |
| 450 °C | 7.67 | 1.86 | 8.85 | 17.00 | 1.45 |
| 580 °C | 14.58 | 1.28 | 11.00 | 15.80 | 1.17 |

[a] ND: not detectable.

with the PtNPs, and thereby on the photovoltaic performance of the pertinent DSSC, is further examined.

Fig. 6 presents the FE-SEM surface images of PtNP/MWCNT film annealed at various temperatures. It can be seen that the image of the film annealed at 110 °C (Fig. 6a) is fainter than those of the film annealed at other temperatures; this may be due to the presence of complete POEM in the composite. The image of the film annealed at 200 °C (Fig. 6b) becomes clearer, because of the partial conversion of $H_2PtCl_6$ to PtNPs and also because of the decomposition of non-conducting POEM. Moreover, MWCNTs on the FTO substrate are distinctly observed (Fig. 6b). The progressive growth in the crystalline sizes of PtNPs is indicated at the temperatures from 390 to 580 °C by the expansion of white dots spread on the substrate (Fig. 6c–e). These results are in consistency with those from the XRD spectra (Table 2). Additionally, the rod-like structures of MWCNTs diminish partially at 450 °C (Fig. 6d), with reference to these structure of the film annealed at 390 °C (Fig. 6c), due to the decomposition of MWCNTs; this observation is also in consistency with the values of $R_{ms}$ obtained from AFM (Table 1). When the annealing temperature reaches to 580 °C, the decomposition of the MWCNTs is complete, as judged by the disappearance of MWCNTs in Fig. 6e.

Since both the crystalline size of PtNPs and the surface morphology of the composite film are affected by the annealing temperature, the surface area and the catalytic ability of the composite film also would be affected; this in turn would affect the performance of the pertinent DSSC. To estimate the actual catalytic surface areas of the films annealed at different temperatures, CVs were obtained for the films annealed at these temperatures. Fig. 7

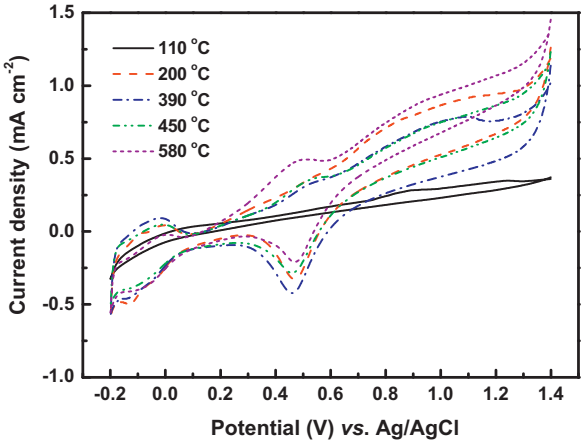


**Fig. 7.** CV curves of PtNP/MWCNT-CEs obtained in 0.5 M $H_2SO_4$, at the scan rate of 50 mV $s^{-1}$.

shows the CVs of the CEs with the films annealed at various temperatures. The potential of the electrode was swept from −0.2 to 1.4 V (*vs.* Ag/AgCl), at the scan rate of 50 mV $s^{-1}$ in the aqueous medium of 0.5 M $H_2SO_4$ [24]. The geometrical surface area ($A_g$) of the PtNP/MWCNT film was 2.25 $cm^2$. The real surface area ($A_r$) of the PtNP/MWCNT film was estimated by integrating the charges under the anodic and cathodic peaks of the CV within the range of −0.2 to 0.2 V (*vs.* Ag/AgCl), followed by subtracting the charge

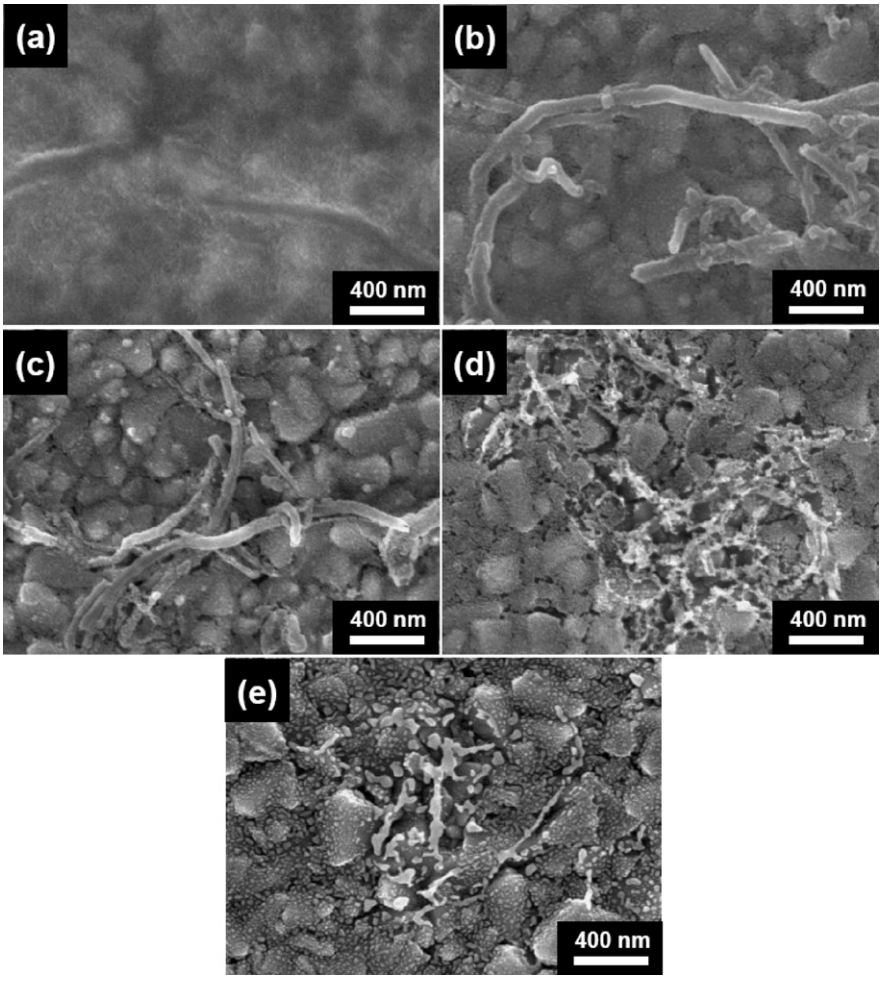


**Fig. 6.** Plane view FE-SEM images of the PtNP/MWCNT-CEs annealed at (a) 110, (b) 200, (c) 390, (d) 450, and (e) 580 °C.

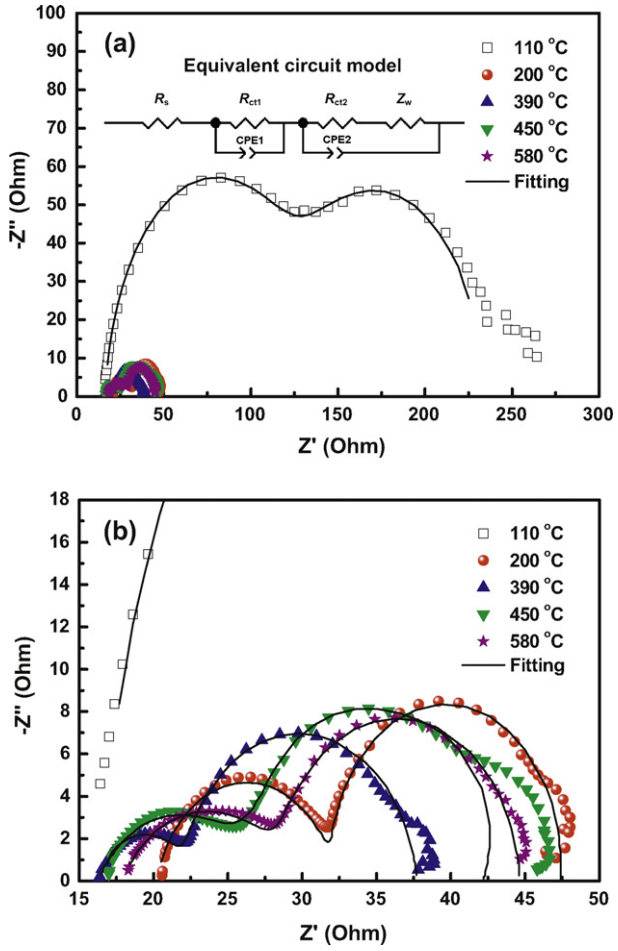


**Fig. 8.** (a) EIS spectra of the DSSCs with PtNP/MWCNT-CEs annealed at 110, 200, 390, 450, and 580 °C; (b) the magnified version of the spectra at the low impedance range.

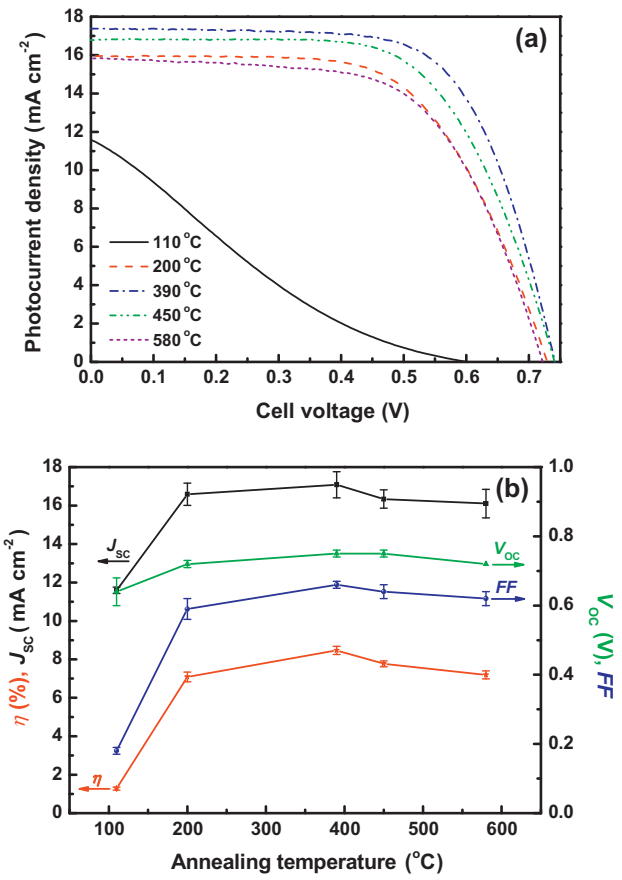


**Fig. 9.** (a) Photocurrent density–voltage characteristics of the DSSCs with PtNP/MWCNT-CEs annealed at different temperatures; (b) photovoltaic parameters of the DSSCs as functions of annealing temperatures of their PtNP/MWCNT-CEs, obtained at 100 mW cm$^{-2}$.

associated with the double layer in the corresponding range of potentials. In addition, a conversion factor of 210 μC cm$^{-2}$ was used for the calculation. The values of $A_r/A_g$ for the films annealed at 200, 390, 450, and 580 °C were found to be 2.16, 2.57, 1.86, and 1.28, respectively (Table 2). The rougher the surface of the film, the higher the catalytic ability of the film [23]; the PtNP/MWCNT-CE annealed at 390 °C is expected to show the highest catalytic ability, due to its highest surface area (Table 2). EIS data were obtained for the DSSCs with the PtNP/MWCNT-CEs annealed at various temperatures. The EIS spectra were obtained at frequencies ranging from 65 kHz to 0.01 Hz, under an illumination of 100 mW cm$^{-2}$. The EIS represent the interfacial charge-transfer resistance at the CE and the electrolyte ($R_{ct1}$), the interfacial charge-transfer resistance at the dye-adsorbed photoanode and the electrolyte ($R_{ct2}$), and the resistance of Warburg diffusion in the electrolyte ($Z_w$). The main effect is expected for $R_{ct1}$, because only the CEs differ in the DSSCs. Fig. 8a shows the EIS spectra of the DSSCs with PtNP/MWCNT-CEs annealed at 110, 200, 390, 450, and 580 °C and Fig. 8b shows the magnified version of the spectra at the low impedance range. The EIS shows significant variations in the $R_{ct1}$ values. The values of $R_{ct1}$, $R_{ct2}$, and $Z_w$ were obtained by fitting the EIS spectra with an equivalent circuit model, which is shown in the inset of Fig. 8a. The $R_{ct1}$ value of the DSSC with the CE annealed at 390 °C is 5.73 Ω; this is the smallest resistance among all obtained for other cells, which are 108.00, 11.93, 8.85, and 11.00 Ω for the annealing temperatures of 110, 200, 450, and 580 °C, respectively (Table 2). This tendency is consistent with the tendency of $A_r/A_g$ (Table 2). On the other hand, the values of $R_{ct2}$ for the DSSCs are almost the same, except in the case of DSSC at 110 °C ($R_{ct2}$ = 111.20 Ω). This largest $R_{ct1}$ is due to the non-conducting POEM coexisting in the film of PtNP/MWCNT, as can be seen by its TGA trace (Fig. 2) and in the SEM image of Fig. 6a. Additionally, the $Z_w$ shows the smallest semicircles, referring to smallest resistances of Warburg diffusion in the electrolyte for all the cells; this is expected as the electrolyte is the same for all the cells.

As $R_{ct1}$ dominated in the EIS data, exchange current density values ($J_0$) for the reduction of $I_3^-$ were calculated from the values of $R_{ct1}$, using the following equation [7]:

$$J_0 = \frac{RT}{nFR_{ct1}} \quad (3)$$

where $F$ is the Faraday constant and $n$ is the number of electrons transferred at the CE for the following electrochemical reaction ($n$ = 2):

$$I_3^- + 2e^- \leftrightarrow 3I^- \quad (4)$$

The highest $J_0$ value of 2.24 mA cm$^{-2}$ obtained for the PtNP/MWCNT-CE annealed at 390 °C (Table 2) indicates the best $I_3^-$ reduction at this CE.

To realize the performances of DSSCs assembled with the PtNP/MWCNT-CEs annealed at 110, 200, 390, 450, and 580 °C, photocurrent density–voltage ($J$–$V$) characteristics of these cells were obtained, at 100 mW cm$^{-2}$ (Fig. 9a). The fill factor (FF) of the DSSC with the CE annealed at 110 °C is 0.18 ± 0.01 (Table 3); this lowest FF is apparently due to the unfavorable

**Table 3**
Photovoltaic parameters of the DSSCs with PtNP/MWCNT-CEs annealed at various temperatures, obtained at 100 mW cm$^{-2}$. The values at each temperature are average values of three cells.

| Annealing temp. | $J_{SC}$ (mA cm$^{-2}$) | $V_{OC}$ (V) | FF | $\eta$ (%) |
|---|---|---|---|---|
| 110 °C | 11.59 ± 0.16 | 0.64 ± 0.04 | 0.18 ± 0.01 | 1.28 ± 0.08 |
| 200 °C | 16.59 ± 0.58 | 0.72 ± 0.01 | 0.59 ± 0.03 | 7.09 ± 0.25 |
| 390 °C | 17.08 ± 0.68 | 0.75 ± 0.01 | 0.66 ± 0.01 | 8.47 ± 0.21 |
| 450 °C | 16.34 ± 0.48 | 0.75 ± 0.01 | 0.64 ± 0.02 | 7.77 ± 0.15 |
| 580 °C | 16.10 ± 0.74 | 0.72 ± 0.00 | 0.62 ± 0.02 | 7.19 ± 0.21 |

electron-transfer in the PtNP/MWCNT composite film containing non-conducting POEM. A very low short-circuit current density ($J_{SC}$), open-circuit voltage ($V_{OC}$), and power-conversion efficiency ($\eta$) of 11.59 ± 0.16 mA cm$^{-2}$, 0.64 ± 0.04 V, and 1.28 ± 0.08%, respectively, are obtained for the DSSC with the CE annealed at 110 °C (Table 3). When the annealing temperature is increased to 200 °C, the $J_{SC}$, $V_{OC}$, and $\eta$ of the pertinent DSSC are 16.59 ± 0.58 mA cm$^{-2}$, 0.72 ± 0.01 V, and 7.09 ± 0.25%, respectively; this enhancement in the performance of the DSSC is attributed to the progressive formation of PtNPs, which could provide more catalytic sites for the $I_3^-$ reduction, with reference to those in the case of the DSSC with the CE annealed at 110 °C. The $H_2PtCl_6$ is completely converted to PtNPs at the annealing temperature of 390 °C (see Fig. 4). Moreover, the decomposition of non-conducting POEM occurs in the range of 200–390 °C (see Fig. 2), and this accompanies an enhancement in the catalytic ability of the PtNP/MWCNT-CE. Thus the best $\eta$ of 8.47 ± 0.21% was obtained for the DSSC with the PtNP/MWCNT-CE annealed at 390 °C. Furthermore, the DSSCs show a decrease in their performance at the annealing temperatures higher than 390 °C. This is due to the decomposition of MWCNTs, which decreases the value of $R_{ms}$ (Table 1) and due to the growth of PtNPs, which decreases the value of $A_r/A_g$ (Table 2). Decomposition of MWCNTs reduces the surface roughness of the PtNP/MWCNT-CE and renders small surface area for the $I_3^-$ reduction. Growth of PtNPs also causes a decrease in the surface area of the film and thereby reduces the catalytic ability of the film. Therefore, the efficiencies of the DSSCs have decreased to 7.77 ± 0.15% and 7.19 ± 0.21% at the temperatures of 450 and 580 °C, respectively (Table 3). Fig. 9b shows the photovoltaic parameters of the DSSCs as functions of annealing temperatures of their PtNP/MWCNT-CEs. According to Fig. 9b, the optimal annealing temperature of PtNP/MWCNT-CE is 390 °C, in terms of $J_{SC}$ and $\eta$ of the corresponding cell. Fig. 10 shows that the $J_{SC}$ (17.08 ± 0.68 mA cm$^{-2}$) and the $\eta$ (8.47 ± 0.21%) of the DSSC with the PtNP/MWCNT-CE annealed at 390 °C are higher than those of the cell fabricated with a bare PtNP-CE annealed at the same temperature ($J_{SC}$ = 16.56 ± 0.31 mA cm$^{-2}$, $\eta$ = 7.41 ± 0.24%). The high performance of the cell with PtNP/MWCNT-CE is ascribed to the MWCNTs which provide a rough surface to the CE, thereby providing a high catalytic ability to it.

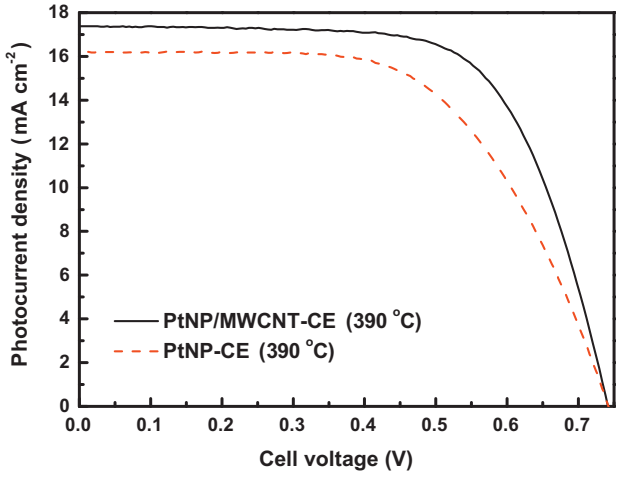


**Fig. 10.** Photocurrent density–voltage characteristics of the DSSCs fabricated with the PtNP/MWCNT-CE and with the bare PtNP-CE, in which both CEs were annealed at 390 °C; the DSSCs were illuminated at 100 mW cm$^{-2}$.

## 4. Conclusions

The CEs with nanocomposite films of PtNP/MWCNT were prepared at different annealing temperatures (110–580 °C) using a home-made polymeric dispersant, POEM. The thus prepared CEs were used to fabricate highly efficient DSSCs. The masses of the components of the film, i.e., POEM, $H_2PtCl_6$, and MWCNTs showed variations at different annealing temperatures, as characterized by TGA. This variation is consistent with the formation of PtNPs from $H_2PtCl_6$ and with the decompositions of both POEM and MWCNTs. The crystalline sizes of PtNPs have increased with the increase in the annealing temperature, and the surface roughness of the nanocompsite film has decreased from 390 °C. All these phenomena rendered different catalytic abilities for the PtNP/MWCNT-CEs, annealed at different temperatures, for the $I_3^-$ reduction and further affected the photovoltaic performance of the DSSCs with the corresponding CEs. The DSSC with the PtNP/MWCNT-CE, annealed at 390 °C showed the highest power-conversion efficiency of 8.47 ± 0.21%. The superior performance of the DSSC is attributed to the fine dispersion of the inorganic component by POEM, to the formation of PtNP with a moderate crystalline size, to the surface roughness of the pertinent film, and to the complete decomposition of the non-conducting POEM in the film of PtNP/MWCNT.

## Acknowledgements

This work was financially supported by the National Science Council (NSC) of Taiwan. A part of this work was also supported by the Academia Sinica, Nangkang, Taiwan.

## References

[1] B. O'Regan, M. Grätzel, Nature 353 (1991) 737–740.
[2] N. Papageorgiou, Y. Athanassov, M. Armand, P. Bonhôte, H. Pettersson, A. Azam, M. Grätzel, J. Electrochem. Soc. 143 (1996) 3099–3108.
[3] C.H. Yoon, R. Vittal, J. Lee, W.S. Chae, K.J. Kim, Electrochim. Acta 53 (2008) 2890–2896.
[4] X. Fang, T. Ma, G. Guan, M. Akiyama, T. Kida, E. Abe, J. Electroanal. Chem. 570 (2004) 257–263.
[5] S. Ito, N.L.C. Ha, G. Rothenberger, P. Liska, P. Comte, S.M. Zakeeruddin, P. Péchy, M.K. Nazeeruddin, M. Grätzel, Chem. Commun. (2006) 4004–4006.
[6] N. Papageorgiou, W.F. Maier, M. Grätzel, J. Electrochem. Soc. 144 (1997) 876–884.
[7] L.Y. Lin, P.C. Nien, C.P. Lee, K.W. Tsai, M.H. Yeh, R. Vittal, K.C. Ho, J. Phys. Chem. C 114 (2010) 21808–21815.
[8] K. Sun, B. Fan, J. Ouyang, J. Phys. Chem. C 114 (2010) 4237–4244.
[9] S. Ahmad, J.H. Yum, Z. Xianxi, M. Grätzel, H.J. Butt, M.K. Nazeeruddin, J. Mater. Chem. 20 (2010) 1654–1658.
[10] J.D.R. Mayhew, D.J. Bozym, C. Punckt, I.A. Aksay, ACS Nano 4 (2010) 6203–6211.
[11] Z. Wu, Z. Chen, X. Du, J.M. Logan, J. Sippel, M. Nikolou, K. Kamaras, J.R. Reynolds, D.B. Tanner, A.F. Hebard, A.G. Rinzler, Science 305 (2004) 1273–1276.
[12] X. Mei, J. Ouyang, Carbon 48 (2010) 293–299.
[13] W.J. Lee, E. Ramasamy, D.Y. Lee, J.S. Song, ACS Appl. Mater. Interfaces 1 (2009) 1145–1149.
[14] S.I. Cha, B.K. Koo, S.H. Seo, D.Y. Lee, J. Mater. Chem. 20 (2010) 659–662.
[15] B. Fan, X. Mei, K. Sun, J. Ouyang, J. Appl. Phys. Lett. 93 (2008) 143103.
[16] X. Mei, S.J. Cho, B. Fan, J. Ouyang, Nanotechnology 21 (2010) 395202.
[17] H. Han, U. Bach, Y.B. Cheng, R.A. Caruso, C. MacRae, Appl. Phys. Lett. 92 (2009) 103102.
[18] K.C. Huang, Y.C. Wang, R.X. Dong, W.C. Tsai, K.W. Tsai, C.C. Wang, Y.H. Chen, R. Vittal, J.J. Lin, K.C. Ho, J. Mater. Chem. 20 (2010) 4067–4073.

[19] J.G. Chen, V. Suryanarayanan, K.M. Lee, K.C. Ho, Sol. Energy Mater. Sol. Cells 91 (2007) 1432–1437.
[20] M.G. Kang, N.G. Park, K.S. Ryu, S.H. Chang, K.J. Kim, Sol. Energy Mater. Sol. Cells 90 (2006) 574–581.
[21] T. Teranishi, M. Hosoe, T. Tanaka, M. Miyake, J. Phys. Chem. B 103 (1999) 3818–3827.
[22] W. Wang, X. Chen, Q. Cai, G. Mo, L.S. Jiang, K. Zhang, Z.J. Chen, Z.H. Wu, W. Pan, Eur. Phys. J. B 65 (2008) 57–64.
[23] C.H. Zhou, Y. Yang, J. Zhang, S. Xu, S.J. Wu, H. Hu, B.L. Chen, Q.D. Tai, Electrochim. Acta 54 (2009) 5320–5325.
[24] G.S. Attard, P.N. Bartlett, N.R.B. Coleman, J.M. Elliott, J.R. Owen, J.H. Wang, Science 278 (1997) 838–840.